



Semnan University

Mechanics of Advanced Composite Structures

journal homepage: <http://MACS.journals.semnan.ac.ir>

A Meshfree Approach for Bending Analysis of Porous Rectangular FGM Plate Resting on Elastic Foundation

R. Kumar ^{a*}, C. Kumar ^b, M. Singh ^c, J. Damania ^a, J. Singh ^d, J. Singh ^d

^a Department of Mechanical Engineering, Sardar Vallabhbhai National Institute of Technology, Surat-395007, India

^b Department of Mechanical Engineering, BIT Mesra, off-campus, Patna-80014, India

^c Institute of Business Management, GLA University, Mathura- 281406, India

^d Department of Mechanical Engineering, MMMUT, Gorakhpur-273010, India

KEYWORDS

FGM plate;
Bending;
MQ-RBF;
Patch load;
Elastic foundation.

ABSTRACT

This study explores the bending analysis of porous functionally graded material (FGM) rectangular plate resting on two parameters elastic foundation based on the higher-order shear deformation theory (HSDT) and subjected to various types of transverse load. The material properties of porous FGM rectangular plates are assumed to be graded in the thickness direction according to modified power-law distribution in terms of the porosity fractions and grading index. The energy principle develops governing differential equations (GDEs) of the plate. The derived formulation is implemented numerically using the strong formulation, and the multiquadric radial basis function (MQ-RBF) based meshfree method for discretizing the GDEs. The MQ-RBF improved by modifying the radial distance between the interpolation. A code has been developed in MATLAB (2019) to obtain the results. The influence of the span to thickness ratio, aspect ratio, transverse loading type, porosity fraction, grading index, and elastic foundation coefficients on the bending response of porous FGM rectangular plate. New numerical results can provide benchmarks for future analyses of porous FGM plates on elastic foundations.

1. Introduction

Generally, models originating from practical applications in industry and engineering do not have an exact solution, or it is exorbitant to be implemented and actualized. Thus, such intentions are unavoidable depending on computational calculations, mainly numerical methods.

The significant increase in the industrial use of composites constructions necessitated the development of various methods for analyzing structures made of these materials. Several analytical methods are used to solve engineering problems, but these can be applied only for problems with simple geometry and loading. With the advent of the fast computational facility, numerical methods have become a valuable tool for analyzing complex engineering problems. The basic advantage of the numerical methods is that they can handle real geometrical shapes and loadings, as distinct from somewhat limited shapes and loading, which analytical methods can

handle. Most used numerical methods are the finite difference (FDM), finite element (FEM), and differential quadrature methods (DQM). FEM is now widely used in handling problems with complex geometry. However, this becomes expensive and time-consuming to discretize the complex geometry domain. In addition, in the case of large deformations, considerable accuracy is lost because of element distortion.

In the recent past, a more general method known as Meshless or Meshfree Method has avoided the mesh generation problem. These meshless methods have the ability of a numerical simulation process being constructed entirely from a set of nodes avoiding any pre-specified connectivity between the nodes. This has created the interest and motivation of researchers to investigate the various engineering problems using meshfree methods.

Recently detailed elucidation of various types of meshfree methods can be discussed by Chen Jiun-Shyan et al. [1]. Meshfree methods formulation developed under two categories

* Corresponding author. Tel.: +917543934007
E-mail address: rahul22mech@gmail.com

which are known as strong form-based formulation such as radial basis collocation method [2], [3], and weak form-based formulation such as radial point interpolation method [4]. The meshfree method based on the strong form formulation attracts many researchers due to its high accuracy and fast convergence rate, and it is implemented easily. The time cost is significantly reduced. In the previous 25 years, the strong form formulation of the meshfree method, which depends on the RBFs, has gotten alluring for solving partial differential equations (PDEs). RBF based meshfree method is truly meshfree nature that can directly discretize GDE's of any order, along with their boundary conditions. The foundation thought of RBF interpolation was introduced by Hardy[5] to appraise in scattered data sets. After two decades, Kansa [3] pioneered the concept of solving PDEs utilized by multiquadric RBF. Franke [6] investigated the assessment of RBFs for scattered data interpolation in terms of time cost, accuracy, and simplicity of usage. Functionally graded materials (FGMs), considered heterogeneous composite material has drawn considerable attention of the research community due to spatial variation of material properties in specific direction through appropriate volume fractions. This demanding feature of FGMs opens wide range of applications in many engineering applications such as aerospace, aircraft engineering, nuclear reactors, civil, shipbuilding industries, automotive, biomechanical, etc. Hence, numerous works based on FGMs has received much attention from researcher's community. During application, bending analysis of FGMs rectangular plate under the various types of transverse loading plays a significant role for better safety and reliability at high temperature conditions. Carrera et al. [7] investigated bending analysis of FGM plate by using finite element solution. Zenkour [8] presented a bending analysis of the FGM plate via sinusoidal HSDT. Mantari [9] introduced a new HSDT for the bending response of the FGM plate by using a Navier-type analytical solution. Kumar et al. [10] proposed two new HSDTs for the bending analysis of FGM plate via the Wendland RBF method. Neves et al. [11] used sinusoidal plate formulation via RBF for the bending analysis of the FGM plate. Mechab et al.[12] used two variable refined plate theory for the bending response of FGM plate. Neya [13] investigated the exact solution for the bending analysis of the FGM plate. Meksi et al. [14] studied the bending and free vibration response of Winkler or Pasternak elastically supported FGM plate via neutral surface position and first-order shear deformation theory (FSDT). Recently, investigations of FGM plates with porosity effects

have been identified as an interesting field. According to the comprehensive literature survey, it can be found that there are scarcely any reported studies in this field. Yahia et al. [15] investigated wave propagation in porous FGM plates via various HSDTs. Benferhat et al. [16] investigated bending analysis of porous FGM plate via four variables new HSDT. Kim et al. [17] used three types of porosity distribution for the bending, buckling and free vibration of porous FGM micro-plate. Akbaş [18] examined vibration and statics analysis of porous FGM plate by using odd and even porosity distributions. Mechab et al. [19] examined free vibration analysis of Winkler Pasternak elastic elastically supported porous FGM nanoplate via two-variable refined plate theories. Gupta and Talha, [20] investigated flexural and vibration response of porous FGM plate using sinusoidal hyperbolic inverse HSDT. Rezaei et al. [21] investigated natural frequency of porous FGM plate using four variables refined theory. Chen et al. [22] investigated bending and buckling analysis of porous FGM plate via three types of porosity distributions.

Recently, mesh-free methods have been considered for analyzing FGM structures subjected to various types of loading to avoid the drawbacks of mesh-based methods such as distortion of meshes causing inaccurate and unstable solutions and high costs and more time taken in creating remeshing can be avoided. Meshfree methods examine the problem domain using scattered nodes [23]. Ferreira et al. [24] investigated static analysis of FGM plate using TSDT with multiquadric (MQ) RBF-based meshless method. Dai et al.[25] investigated the analyses of FGM plate based on the radial point interpolation meshfree method. Wu et al.[26] proposed a meshless collocation and Element-Free Galerkin methods for the quasi-3D analyses of single and multilayered FGM plates. [27] applied the RBF-based meshfree method for the quasi-3D analysis of FGM plates based on the CUF. It was concluded that the normal transverse stress should not be neglected for the thin plates. Xiang and Kang [28] used the thin-plate spline RBF technique with the n th-order shear deformation theory for the bending analysis of FGM plates. Xiang and Kang [29] used thin-plate spline RBF to discretize GDE based on the meshfree method. Five HSDT models have been considered for the statics analysis of the FGM plate. To the author's knowledge, few results have been reported for the porous FGM rectangular plates resting on elastic foundations. Another novel contribution of the present work is the analysis of porous FGM plate for different types of patch load resting on two parameters elastic foundation by using MQ-RBF based meshfree method.

2. Mathematical Formulation

Porous FGM rectangular plate constitution by a combination of ceramics and metals is shown in Fig. 1. The length of porous FGM plate is 'a' width 'b,' and thickness 'h' is taken with the coordinates x, y, and z directions.

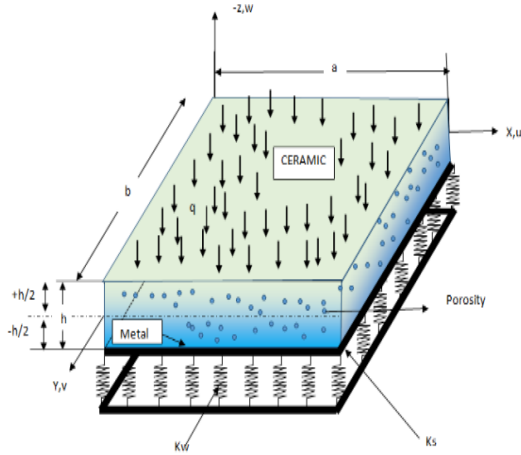


Fig. 1. Geometry of the functionally graded materials plate resting on elastic foundations

2.1. Displacement Field

The displacement field based on the five variables HSDT can be expressed as [30]:

$$\begin{aligned} u &= u_0(x, y) - z \frac{\partial w_0(x, y)}{\partial x} + f(z) \phi_x(x, y) \\ v &= v_0(x, y) - z \frac{\partial w_0(x, y)}{\partial y} + f(z) \phi_y(x, y) \\ w &= w_0(x, y) \end{aligned} \quad (1)$$

where $u, v,$ and w are the in-plane and transverse displacements of the plate at any point (x, y, z, t) in $x, y,$ and z directions, respectively. $u_0, v_0,$ and w_0 are the displacements at the mid-plane of the plate at any point (x, y) in $x, y,$ and z directions, respectively. The functions ϕ_x and ϕ_y are the higher order rotations of the normal to the mid-plane due to shear deformation about the y and x axes, respectively. $f(z)$ represents the transverse shear stress functions determining the distribution of the transverse shear strains and stresses along with the thickness.

$f(z)$ is a transverse shear deformation function which is expressed as [30]:

$$f(z) = z \tan^{-1} h \left(\tanh \left(2\pi \left(\frac{z}{h} \right)^2 \right) \right) - \left(\frac{3\pi z}{2} \right) \quad (2)$$

2.2. Strain Displacement Equation

Singh et al. [31] express strain-displacement equations with linear terms:

$$\begin{Bmatrix} \epsilon_{xx} \\ \epsilon_{yy} \\ \gamma_{xy} \\ \gamma_{yz} \\ \gamma_{zx} \end{Bmatrix} = \begin{Bmatrix} \frac{\partial u}{\partial x} \\ \frac{\partial v}{\partial y} \\ \frac{\partial u}{\partial y} + \frac{\partial v}{\partial x} \\ \frac{\partial v}{\partial z} + \frac{\partial w}{\partial y} \\ \frac{\partial u}{\partial z} + \frac{\partial w}{\partial x} \end{Bmatrix} = \begin{Bmatrix} \frac{\partial u_0}{\partial x} - z \frac{\partial^2 w_0}{\partial x^2} + f(z) \frac{\partial \phi_x}{\partial x} \\ \frac{\partial v_0}{\partial y} - z \frac{\partial^2 w_0}{\partial y^2} + f(z) \frac{\partial \phi_y}{\partial y} \\ \frac{\partial u_0}{\partial y} + \frac{\partial v_0}{\partial x} - 2z \frac{\partial^2 w_0}{\partial x \partial y} + f(z) \frac{\partial \phi_x}{\partial y} + f(z) \frac{\partial \phi_y}{\partial x} \\ \frac{\partial f(z)}{\partial z} \phi_y \\ \frac{\partial f(z)}{\partial z} \phi_x \end{Bmatrix} \quad (3)$$

2.3. Modified Power Law Function

Effective material properties of the FGM rectangular plate through the plate thickness are assumed to be represented by a modified power-law and are given as [17].

$$E(z) = \left([E_c - E_m] \left(\frac{2z+h}{2h} \right)^n + E_m \right) \left(1 - \left(P \cos \left(\frac{\pi z}{h} \right) \right) \right), \quad (4)$$

$(-h/2 \leq z \leq h/2)$

The subscripts m and c refer to metal and ceramic, respectively, 'n' is the grading index, and P is the porosity index ($0 < P < 1$)

2.4. Constitutive relations of FGM structures

The 2-D constitutive relations can be expressed as [32]:

$$\begin{Bmatrix} \sigma_{xx} \\ \sigma_{yy} \\ \sigma_{xy} \\ \sigma_{yz} \\ \sigma_{zx} \end{Bmatrix} = \begin{bmatrix} \bar{Q}_{11} & \bar{Q}_{12} & 0 & 0 & 0 \\ \bar{Q}_{12} & \bar{Q}_{22} & 0 & 0 & 0 \\ 0 & 0 & \bar{Q}_{66} & 0 & 0 \\ 0 & 0 & 0 & \bar{Q}_{44} & 0 \\ 0 & 0 & 0 & 0 & \bar{Q}_{55} \end{bmatrix} \begin{Bmatrix} \epsilon_{xx} \\ \epsilon_{yy} \\ \gamma_{xy} \\ \gamma_{yz} \\ \gamma_{zx} \end{Bmatrix} \quad (5)$$

$\bar{Q}_{i,j}$ is plane stress-reduced stiffness and is given below [33]:

$$\begin{aligned} \bar{Q}_{11} = \bar{Q}_{22} &= \frac{E(z)}{(1-\nu^2)}, \quad \bar{Q}_{12} = \frac{\nu E(z)}{(1-\nu^2)}, \\ \bar{Q}_{44} = \bar{Q}_{55} = \bar{Q}_{66} &= \frac{E(z)}{2(1+\nu)} \end{aligned} \quad (6)$$

2.5. Governing Differential Equation

Using the energy principle, potential energy can be expressed as:

$$V = U + U_f - W \quad (7)$$

where U =strain energy, U_f =strain energy of the elastic foundation, and W = work done by the distributed transverse load

The strain energy (U) of the FGM plate is expressed by Akavci, S.S [31]:

$$U = \frac{1}{2} \int_{-\frac{h}{2}}^{\frac{h}{2}} \int_A (\sigma_{xx}\epsilon_{xx} + \sigma_{yy}\epsilon_{yy} + \sigma_{xy}\gamma_{xy} + \sigma_{yz}\gamma_{yz} + \sigma_{xz}\gamma_{xz}) dz dA \quad (8)$$

The strain energy of the elastic foundation (Uf) can be expressed as [35]:

$$U_f = \frac{1}{2} \left(\int_A kw(w^2) - ks \left[\left(\frac{\partial w}{\partial x} \right)^2 + \left(\frac{\partial w}{\partial y} \right)^2 \right] dA \right) \quad (9)$$

Work done by the distributed transverse load is expressed by:

$$W = \int_A q_z w dA \quad (10)$$

in which q_z is the transverse load applied on the FGM plate. The forces and moments are expressed as,

$$\left(N_{ij}, M_{ij}, M_{ij}^f \right) = \int_{-h/2}^{+h/2} (\sigma_{ij}, z\sigma_{ij}, f(z)\sigma_{ij}) dz \quad (11)$$

$$\left(Q_x^f, Q_y^f \right) = \int_{-h/2}^{+h/2} (\sigma_{xz}, \sigma_{yz}) \left(\frac{\partial f(z)}{\partial z} \right) dz \quad (12)$$

The stiffness coefficients of the FGM plates can be written as:

$$A_{ij}, B_{ij}, D_{ij}, E_{ij}, F_{ij}, H_{ij} = \int_{-h/2}^{h/2} \left\{ \left(Q_{ij}^{cm} \right) (1, z, z^2, f(z), z f(z), f^2(z)) \right\} dz \quad (13)$$

$$Q_{ij}^{cm} = \left(\left[Q_{ij}^c - Q_{ij}^m \right] \left(\frac{2z+h}{2h} \right)^n + Q_{ij}^m \right) \left(1 - \left(P \cos \left(\frac{\pi z}{h} \right) \right) \right)$$

$$A_{ij} = \int_{-h/2}^{h/2} \left\{ \left(Q_{ij}^{cm} \right) \left(\frac{\partial f(z)}{\partial z} \right)^2 \right\} dz \quad (14)$$

The coefficients of $\delta u_0, \delta v_0, \delta w_0, \phi_x$ and ϕ_y can be expressed as:

$$\delta u_0 : \frac{\partial N_{xx}}{\partial x} + \frac{\partial N_{xy}}{\partial y} = 0 \quad (15)$$

$$\delta v_0 : \frac{\partial N_{xy}}{\partial x} + \frac{\partial N_{yy}}{\partial y} = 0 \quad (16)$$

$$\delta w_0 : \frac{\partial^2 M_{xx}}{\partial x^2} + \frac{\partial^2 M_{yy}}{\partial y^2} + 2 \frac{\partial^2 M_{xy}}{\partial x \partial y} \quad (17)$$

$$-q_z + kw w_0 - ks \left(\frac{\partial^2 w_0}{\partial x^2} + \frac{\partial^2 w_0}{\partial y^2} \right) = 0$$

$$\delta \phi_x : \frac{\partial M_{xx}^f}{\partial x} + \frac{\partial M_{xy}^f}{\partial y} - Q_x^f = 0 \quad (18)$$

$$\delta \phi_y : \frac{\partial M_{xy}^f}{\partial x} + \frac{\partial M_{yy}^f}{\partial y} - Q_y^f = 0 \quad (19)$$

2.6. Boundary conditions

Three boundary conditions, namely all edges simply-supported plate (SS), all edges clamped supported plate (CC), two simply supported and two clamped (CS), are considered in the present analysis, which is as follows [36].

2.6.1 Simply supported plate (SS) is expressed as

$$\begin{aligned} x=0, a: N_{xx}=0, v_0=0, w_0=0, M_{xx}=0, \phi_y=0 \\ y=0, b: u_0=0, N_{yy}=0, w_0=0, \phi_x=0, M_{yy}=0 \end{aligned} \quad (20)$$

2.6.2. Clamped plate (CC) is expressed as

$$\begin{aligned} x=0, a: u_0=0, v_0=0, w_0=0, \phi_x=0, \phi_y=0 \\ y=0, b: u_0=0, v_0=0, w_0=0, \phi_x=0, \phi_y=0 \end{aligned} \quad (21)$$

The SC is the combination of the simply supported (SS) and clamped (CC) boundary conditions taken in the present investigation.

3. Solution Methodology

The GDEs are expressed in terms of displacement using MQRBF. MQRBF formulation works on the interpolation of scattered data over the entire domain. Franke [6] has ranked MQRBF as the best interpolation method based on its accuracy, execution time, and ease of implementation. Several other kinds of literature are also available showing the applicability of MQRBF.

The GDE (15-19) and boundary conditions (20-21) are discretized using MQ-RBF. The radial distance between nodes can interpolate the variable. The solution of the linear governing differential Eqs (15) - (19) is assumed in terms of MQ-RBF for nodes 1: N, as;

$$u_0, v_0, w_0, \phi_x, \phi_y = \sum_{j=1}^N (\alpha_j^{u_0}, \alpha_j^{v_0}, \alpha_j^{w_0}, \alpha_j^{\phi_x}, \alpha_j^{\phi_y}) g(\|X - X_j\|, c) \quad (22)$$

The radial distance between the nodes for rectangular coordinates is modified so that the aspect ratio starts changing without changing the shape parameters. The expression used for the square plate.

$$r = \|X - X_j\| = \sqrt{(x - x_j)^2 + (y - y_j)^2},$$

has modified as

$$r = \|X - X_j\| = \sqrt{\left(\frac{x - x_j}{a} \right)^2 + \left(\frac{y - y_j}{b} \right)^2},$$

for the rectangular plate where a and b are the length and breadth of the rectangular plate. (MQRBF)

$$g = (r^2 + c^2)^m; \quad c = \alpha \sqrt{\left(\frac{a}{n_x}\right)^2 + \left(\frac{b}{n_y}\right)^2} \quad (23)$$

where $r = \|X - X_j\|$ 'm' and 'c' are shape parameters. n_x and n_y are number of nodes along with the 'a' and 'b' respectively. α is a constant that governs the value of 'c' for interior and boundary nodes.

While utilizing RBFs, several shape parameters need to be determined for better performance. These parameters can generally be determined by numerical examinations for given types of problems [4]. The shape parameter of RBFs affects the solution's accuracy and the discretized partial differential equations (PDEs) conditioning. These two aspects cannot be optimized for each other independently. Therefore, for any problem with a sufficiently smooth solution, an optimal value of the shape parameter will occur, representing a compromise between accuracy and conditioning. Several approximations, however, have been suggested for the selection of shape parameters; most of them are for the multiquadric RBF. Franke [6] has ranked MQRBF as the best interpolation method based on its accuracy, execution time, and ease of implementation. Still, there are no clear-cut guidelines for selecting the shape parameters. Hence it is a matter of further investigation by the researchers.

A MATLAB (2019) code is developed to acquire the solution for the present investigation. Singh et al. [31] present the time required for the solution by different RBFs, and the static problem in MQ-RBF can be expressed as [10].

3.1. Discretization of Governing Differential Equations

The unknown field variables appearing in governing differential equations are assumed in terms of radial basis function as:

$$\begin{aligned} u_0(x, y) &= \sum_{j=1}^N \alpha_j^{u_0} g(\|X - X_j\|, c) \\ v_0(x, y) &= \sum_{j=1}^N \alpha_j^{v_0} g(\|X - X_j\|, c) \\ w_0(x, y) &= \sum_{j=1}^N \alpha_j^{w_0} g(\|X - X_j\|, c) \\ \phi_x(x, y) &= \sum_{j=1}^N \alpha_j^{\phi_x} g(\|X - X_j\|, c) \\ \phi_y(x, y) &= \sum_{j=1}^N \alpha_j^{\phi_y} g(\|X - X_j\|, c) \end{aligned} \quad (24)$$

We finally expressed in compact matrix form the governing differential discretized equations, which are as follows:

$$\left(\begin{bmatrix} [K]_I \\ [K]_B \end{bmatrix}_{5N \times 5N} + \begin{bmatrix} [K]_I \\ [K]_B \end{bmatrix}_F \right) \{\delta\}_{5N \times 1} = \begin{Bmatrix} [F]_L \\ 0 \end{Bmatrix}_{5N \times 1} \quad (25)$$

$$\{\delta\} = \left(\begin{bmatrix} [K]_I \\ [K]_B \end{bmatrix} + \begin{bmatrix} [K]_I \\ [K]_B \end{bmatrix}_F \right)^{-1} \begin{Bmatrix} [F]_L \\ 0 \end{Bmatrix} \quad (26)$$

where

$$[K]_I = \begin{bmatrix} [K^I_{1u}]_{(N,N)} & [K^I_{1v}]_{(N,N)} & [K^I_{1w}]_{(N,N)} & [K^I_{1\phi_x}]_{(N,N)} & [K^I_{1\phi_y}]_{(N,N)} \\ [K^I_{2u}]_{(N,N)} & [K^I_{2v}]_{(N,N)} & [K^I_{2w}]_{(N,N)} & [K^I_{2\phi_x}]_{(N,N)} & [K^I_{2\phi_y}]_{(N,N)} \\ [K^I_{3u}]_{(N,N)} & [K^I_{3v}]_{(N,N)} & [K^I_{3w}]_{(N,N)} & [K^I_{3\phi_x}]_{(N,N)} & [K^I_{3\phi_y}]_{(N,N)} \\ [K^I_{4u}]_{(N,N)} & [K^I_{4v}]_{(N,N)} & [K^I_{4w}]_{(N,N)} & [K^I_{4\phi_x}]_{(N,N)} & [K^I_{4\phi_y}]_{(N,N)} \\ [K^I_{5u}]_{(N,N)} & [K^I_{5v}]_{(N,N)} & [K^I_{5w}]_{(N,N)} & [K^I_{5\phi_x}]_{(N,N)} & [K^I_{5\phi_y}]_{(N,N)} \end{bmatrix}_{(5N \times 5N)} \quad (27)$$

$$[F]_L = \begin{Bmatrix} 0 \\ 0 \\ q \\ 0 \\ 0 \end{Bmatrix}_{5N \times 1} \quad (28)$$

$$[K]_F = \begin{bmatrix} [0] & [0] & [0] & [0] & [0] \\ [0] & [0] & [0] & [0] & [0] \\ [0] & [0] & [K_w w_0 - K_s \left(\frac{\partial^2 w_0}{\partial x^2} + \frac{\partial^2 w_0}{\partial y^2} \right)] & [0] & [0] \\ [0] & [0] & [0] & [0] & [0] \\ [0] & [0] & [0] & [0] & [0] \end{bmatrix}_{(5 \times N \times 5 \times N)} \quad (29.1)$$

$$[K]_B = [0]_{(5 \times NB, 5 \times N)} \quad (29.2)$$

Here, $[K]_I$ represent the stiffness matrix for interior points resulting from LHS of Eq. (17) $[F]_L$ and represents the force matrix resulting from RHS of Eq. (17).

The boundary conditions can be discretized similarly. E.g., simply supported boundary condition at the edge $x=0$ is discretized and finally expressed as:

$$[K]_{b, x=0} \{\delta\} = \{0\} \quad (30)$$

where

$$[K]_{b, x=0} = \begin{bmatrix} [K^{Ib}_{1u}] & [K^{Ib}_{1v}] & [K^{Ib}_{1w}] & [K^{Ib}_{1\phi_x}] & [K^{Ib}_{1\phi_y}] \\ [0]_{nbx_0 \times N} & [K^{Ib}_{2v}] & [0]_{nbx_0 \times N} & [0]_{nbx_0 \times N} & [0]_{nbx_0 \times N} \\ [0]_{nbx_0 \times N} & [K^{Ib}_{2v}] & [K^{Ib}_{3w}] & [0]_{nbx_0 \times N} & [0]_{nbx_0 \times N} \\ [K^{Ib}_{4u}] & [K^{Ib}_{4v}] & [K^{Ib}_{4w}] & [K^{Ib}_{4\phi_x}] & [K^{Ib}_{4\phi_y}] \\ [0]_{nbx_0 \times N} & [K^{Ib}_{2v}] & [0]_{nbx_0 \times N} & [0]_{nbx_0 \times N} & [K^{Ib}_{5\phi_y}] \end{bmatrix}_{(5 \times nbx_0, 5 \times N)} \quad (31)$$

where details terms of $[K]_I$ and $[K]_B$ are given in Appendix-II

Similarly, other boundary conditions at the edges $x=a$, $y=0$, and $y=b$ are discretized. The resulting equation is written in matrix form as:

$$[K]_B \{\delta\} = \{O\} \tag{32}$$

where,

$$[K]_B = \left[\begin{matrix} [K]_{b,y=0} & [K]_{b,x=a} & [K]_{b,y=b} & [K]_{b,x=0} \end{matrix} \right]_{(5 \times N_B, 5 \times N)}^T \tag{33}$$

while discretizing the boundary, corner nodes are considered only once.

The unknown coefficients $\{\delta\}$ are calculated from equation (25) obtained and finally using equations (24), u_0 , v_0 , w_0 , ϕ_x and ϕ_y at desired locations are obtained. Using equation (1), the displacement components, and using equation (5), the stress components are obtained.

4. Results and Discussion

For bending analysis, the equations were solved by developing a computer program using MATLAB (2019) to obtain the results. A simply supported plate has been taken throughout the study. We presented and discussed various numerical examples in this section to verify the effectiveness of the present method. Based on the convergence study, a 15×15 node is used throughout the study. Four types of FGM Plates are used in this study. Their material properties are enumerated in Table 1. Eight types of distributed transverse load are considered for the analysis which is presented. In Fig. 2 in which, the first and second are bi-sinusoidal load and uniformly distributed load, and the remaining all are patch loads in which 4 square patch loads are applied on 4×4 nodes symmetrically, but the location of patch load is moving in every case.:

Table 1. Material properties of FGM plates are following

Types of Functionally graded material		Properties		
		E (GPa)	ρ	ν
FGM-1	(Al)	70	2702	0.3
	(Al2O3)	380	3800	0.3
FGM-2	(Al)	70	2702	0.3
	(ZrO2)	151	3000	0.3
FGM-3	(Ti-6Al-4V)	105.7	4429	0.298
	(aluminum oxide)	320.2	3750	0.26
FGM-4	Stainless steel	201.04	8166	0.3262
	Silicon nitride	348.43	2370	0.2400

The non-dimensional quantities of deflection, stresses, and elastic foundation parameters are taken as:

$$\bar{w} = 10 \frac{E_c h^3}{q_0 a^4} w$$

$$\bar{\sigma}_{xx} = \frac{h}{q_0 a} \sigma_{xx} \left(\frac{a}{2}, \frac{b}{2}, z \right), \quad \bar{\sigma}_{xy} = \frac{h}{q_0 a} \sigma_{xy} (0, 0, z),$$

$$\bar{\sigma}_{xz} = \frac{h}{q_0 a} \sigma_{xz} \left(0, \frac{b}{2}, z \right), \quad \bar{\sigma}_{yz} = \frac{h}{q_0 a} \sigma_{yz} \left(\frac{a}{2}, 0, \frac{h}{6} \right)$$

$$K_s = \frac{ks12(1-\nu^2)}{E_m h^3}, \quad K_w = \frac{k_w12(1-\nu^2)}{E_m h^3}$$

where w indicates the transverse central deflection.

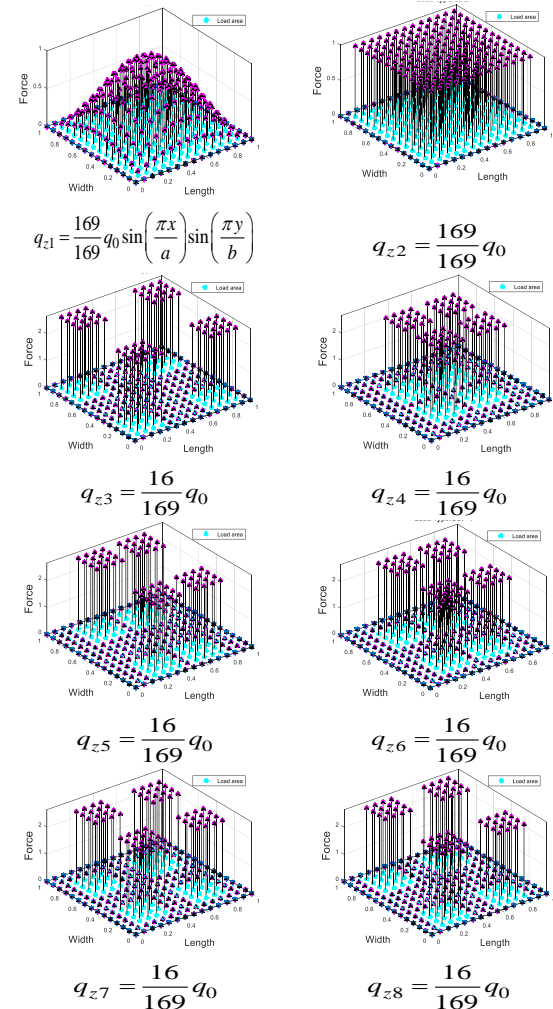


Fig. 2. Various types of distributed transverse loads

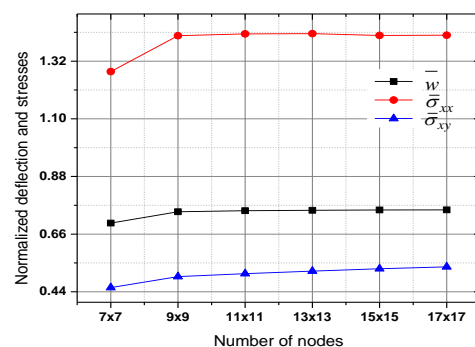


Fig. 3. Convergence study of normalized deflection and stresses of square FGM-1 plate under q_{z1}

Table 2 represents the convergence study of deflections and stresses of square FGM-1 plate under load with $n=2$ and $a/h=10$, which is also depicted in Fig. 3. It can be seen that after 13x13 nodes, normalized deflection and stresses showed good convergence and good agreement with the results reported in the literature [7], [8], [9], [37], [38] and [39]. The results obtained by the present method are compared with the 3D solution given by Carrera et al. [7], and the different percentage at 9x9 nodes is 3.29%, followed by 2.59%, 1.93%, 1.16 and 0.73 at 11x11 nodes, 13x13 nodes, 15x15 nodes, and 17x17 nodes respectively. Fig. 3 shows that the normalized deflection and stresses predict good convergence after 13x13 nodes. So, it is concluded that 15x15 is sufficient for further analysis with computationally inexpensive.

Table 3 represents the normalized deflection and stresses for various values of foundation parameters (K_w , K_s) for square FGM-3 plate under various types of transverse loads. Span to thickness ratio (a/h) =10 with grading index (n)=0.5. It is to be seen that normalized deflection decreases by adding the two parameters elastic foundation for all the distributed transverse loading, and it is also observed that K_s is more dominating than K_w .

Table 4 presents normalized deflection of porous FGM-4 rectangular plate with and without porosity fraction 'P' for different values of two parameters elastic foundation. The aspect ratio (a/b) =2 with grading index(n)=1 and $a/h=10$ under. By increasing the porosity fraction (P), the normalized deflection increases, and by adding the two parameters, elastic foundation normalized deflection decreases. K_s is observed to be more dominating than K_w .

Table 5 presents the effect of aspect ratio on the normalized deflection of porous FGM-4 plate with various span to thickness ratios under q_{z2} loading; by increasing the aspect ratio (a/b) and span to thickness ratio (a/h), normalized deflection decreases, and by increasing porosity fraction, the normalized deflection increases. The

porosity fraction effect dominates the thick plate more than the thin plate.

Table 6 presents the effect of aspect ratio on the normalized deflection of porous FGM-3 plate with various grading indexes under q_{z1} loading. By increasing the aspect ratio (a/b), normalized deflection decreases, and by increasing porosity fraction, P, and grading index, n, the normalized deflection increases, and the effect of porosity fraction is more significant in metals, and the effects are weakened in ceramic phase. Now, the effect of boundary conditions on the normalized deflection of FGM-1 plate ($a/h=100$, q_{z2} , $k_w=0$, $k_s=0$) with different grading indexes ($n=0, 0.5, 1, 2, 5$ and 10) is investigated and shown in Fig. 4. It has been observed that the SS constraint envisages maximum normalized maximum central deflection, and the CC predicts minimum central deflection. All the boundary condition follows the same natures, and by increasing the grading index, normalized central deflection increases.

Fig. 5 represents the effect of span to thickness ratios on the normalized deflection of square FGM-3 plate with different two parameters elastic foundations q_{z1} . Grading index 'n' =1 is taken. It can be seen that the normalized deflection declines from a thin to a thick plate, and by increasing the value of K_w , the normalized deflection decreases less as compared to increasing the value of K_s . Fig.6, Fig. 7 and Fig. 8 represent the stresses along with the thickness of the square FGM-3 plate resting on two parameters elastic foundation q_{z1} . From Fig. 6, a higher value of K_s predicts a maximum $\bar{\sigma}_{xx}$ less, and the low value of K_w predicts a high maximum $\bar{\sigma}_{xx}$. From Fig. 7, it can be seen that $\bar{\sigma}_{xy}$ the entire (K_w , K_s) effect follows the same pattern and predicts maximum at the metal layer. From Fig. 8, the stress $\bar{\sigma}_{xz}$ at the top and bottom satisfied zero conditions and followed parabolic in nature.

Table 2. Convergence and comparison study of normalized deflection and stresses of square FGM-1 plate under q_{z1}

Methods	\bar{w}	$\bar{\sigma}_{xx}$	$\bar{\sigma}_{xy}$	Different %
Carrera et al. [7]	0.757	1.4147	0.5421	----
Wu and Chiu [32]	0.7571	1.4133	0.5421	----
Zenkour [8]	0.7573	1.3954	0.5441	----
Mantari et al.[9]	0.7564	1.394	0.5438	----
Wu and Li [33]	0.7573	1.396	0.5442	----
Thai and Kim [34]	0.7573	1.396	0.5442	----
Present method (9x9 nodes)	0.7452	1.417	0.498	3.29
Present method (11x11 nodes)	0.7494	1.424	0.509	2.59
Present method (13x13 nodes)	0.7509	1.425	0.519	1.93
Present method (15x15 nodes)	0.7522	1.418	0.528	1.16
Present method (17x17 nodes)	0.7526	1.419	0.535	0.73

Table 3. Normalized deflection and stresses of square FGM-3 plate resting on two parameters elastic foundation under various types of transverse loads

(Kw, Ks)	Load Type	\bar{w}_c	$\bar{\sigma}_{xx}\left(\frac{a}{2}, \frac{b}{2}, \frac{h}{2}\right)$	$\bar{\sigma}_{yy}\left(\frac{a}{2}, \frac{b}{2}, \frac{h}{3}\right)$	$\bar{\sigma}_{xy}\left(0, 0, -\frac{h}{3}\right)$
(0,0)	q_{z1}	0.4172	2.3889	1.3883	0.6920
	q_{z2}	0.6525	3.4523	2.0157	1.2363
	q_{z3}	0.3441	1.4348	0.8475	1.0204
	q_{z4}	0.9518	4.9584	2.9178	1.6018
	q_{z5}	0.5671	2.8935	1.3033	1.1479
	q_{z6}	0.7743	4.0089	1.9969	1.4256
	q_{z7}	0.6340	2.8583	1.6811	1.3398
	q_{z8}	0.4664	2.1337	1.1176	1.1078
(100,0)	q_{z1}	0.3706	2.1220	1.2332	0.6147
	q_{z2}	0.5778	3.0264	1.7681	1.1117
	q_{z3}	0.3017	1.1968	0.7090	0.9482
	q_{z4}	0.8438	4.3411	2.5590	1.4225
	q_{z5}	0.4994	2.5082	1.0820	1.0344
	q_{z6}	0.6840	3.4938	1.6994	1.2749
	q_{z7}	0.5585	2.4310	1.4326	1.2130
	q_{z8}	0.4098	1.8138	0.9326	1.0122
(0,100)	q_{z1}	0.1200	0.6858	0.3987	0.2009
	q_{z2}	0.1818	0.8713	0.5122	0.4086
	q_{z3}	0.0868	0.1991	0.1226	0.4536
	q_{z4}	0.2676	1.1724	0.7093	0.4596
	q_{z5}	0.1492	0.6363	0.1435	0.3762
	q_{z6}	0.2101	0.9257	0.3215	0.4348
	q_{z7}	0.1675	0.4876	0.2937	0.4612
	q_{z8}	0.1201	0.3745	0.1482	0.4125
(100,100)	q_{z1}	0.1158	0.6618	0.3848	0.1939
	q_{z2}	0.1751	0.8339	0.4904	0.3972
	q_{z3}	0.0831	0.1797	0.1112	0.4466
	q_{z4}	0.2579	1.1176	0.6774	0.4433
	q_{z5}	0.1432	0.6029	0.1251	0.3656
	q_{z6}	0.2020	0.8805	0.2959	0.4208
	q_{z7}	0.1608	0.4513	0.2725	0.4493
	q_{z8}	0.1151	0.3476	0.1329	0.4034

Table 4. Effect of porosity fraction on the normalized deflection of rectangular porous FGM-4 plate resting elastic foundation

(Kw, Ks)	P=0	P=0.05	P=0.1	P=0.15	P=0.2
(0,0)	0.0940	0.0959	0.0978	0.0998	0.1020
(10,0)	0.0937	0.1165	0.1019	0.1019	0.1016
(100,0)	0.0909	0.1121	0.0944	0.0963	0.0982
(0,10)	0.0902	0.1111	0.0937	0.0955	0.0975
(0,100)	0.0659	0.0668	0.0677	0.0687	0.0697
(100,100)	0.0643	0.0742	0.0661	0.0670	0.0679

Table 5. Effects of aspect ratio and 'P' on the normalized deflection of rectangular FGM-4 plate with various span to thickness ratios

a/h	P	a/b=0.5	a/b=1	a/b=1.5	a/b=2	a/b=3
5	0	2.0386	0.6900	0.2507	0.1024	0.0235
	0.1	2.1461	0.7219	0.2619	0.1069	0.0245
	0.2	2.2683	0.7573	0.2742	0.1119	0.0256
10	0	1.5716	0.6083	0.2278	0.0940	0.0225
	0.1	1.6400	0.6332	0.2370	0.0978	0.0234
	0.2	1.7154	0.6604	0.2470	0.1020	0.0245
20	0	1.4524	0.5875	0.2218	0.0919	0.0219
	0.1	1.5107	0.6106	0.2305	0.0955	0.0227
	0.2	1.5741	0.6357	0.2400	0.0994	0.0237
50	0	1.4178	0.5815	0.2201	0.0925	0.0218
	0.1	1.4731	0.6041	0.2287	0.0961	0.0227
	0.2	1.5330	0.6286	0.2379	0.0999	0.0236
100	0	1.4124	0.5806	0.2199	0.0990	0.0219
	0.1	1.4673	0.6032	0.2284	0.1024	0.0227
	0.2	1.5266	0.6276	0.2376	0.1060	0.0236

Table 6. Effects of aspect ratio and 'P' on the normalized deflection of rectangular FGM-3 plate with various grading indexes

'n'	'P'	a/b=0.5	a/b=1	a/b=1.5	a/b=2	a/b=3
0	0	0.8125	0.3037	0.1145	0.0484	0.0122
	0.1	0.8478	0.3160	0.1191	0.0503	0.0127
	0.2	0.8868	0.3294	0.1241	0.0524	0.0132
1	0	1.3052	0.4911	0.1856	0.0785	0.0198
	0.1	1.3645	0.5121	0.1935	0.0818	0.0207
	0.2	1.4303	0.5353	0.2021	0.0854	0.0216
2	0	1.5056	0.5635	0.2128	0.0900	0.0228
	0.1	1.5723	0.5870	0.2216	0.0936	0.0237
	0.2	1.6464	0.6127	0.2311	0.0977	0.0247
5	0	1.7109	0.6313	0.2376	0.1003	0.0255
	0.1	1.7844	0.6563	0.2469	0.1042	0.0266
	0.2	1.8658	0.6836	0.2570	0.1084	0.0279
10	0	1.8643	0.6855	0.2577	0.1087	0.0277
	0.1	1.9423	0.7117	0.2674	0.1128	0.0290
	0.2	2.0288	0.7403	0.2779	0.1172	0.0306

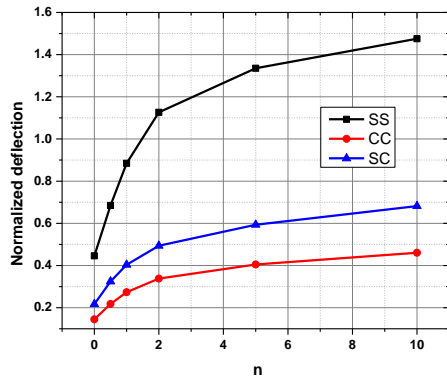


Fig. 4. Normalized deflection of FGM-1 plates under different boundary conditions

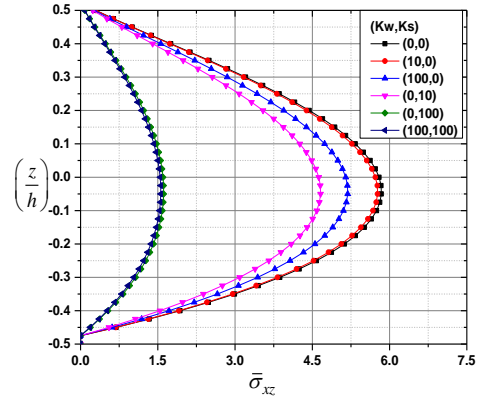


Fig. 8. Effect of the span to thickness ratio on FGM-3 plate resting on elastic foundation

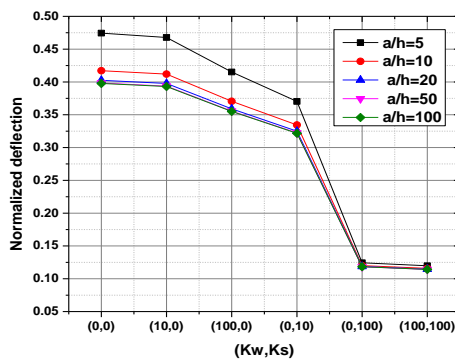


Fig. 5. Effect of span to thickness ratio on the normalized deflection of FGM-3 plate resting on elastic foundation

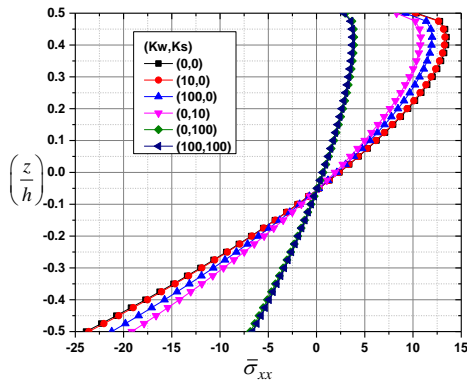


Fig. 6. Effect of the span to thickness ratio on FGM-3 plate resting on elastic foundation

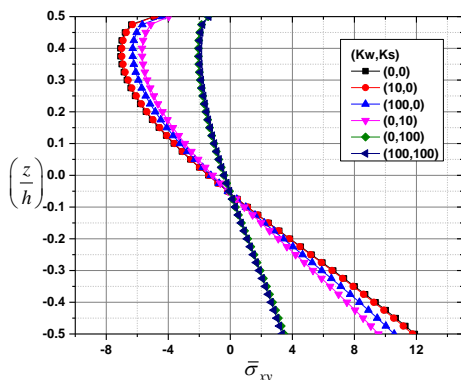


Fig. 7. Effect of the span to thickness ratio on FGM-3 plate resting on elastic foundation

5. Conclusions

In the present paper, the equivalent five variables inverse hyperbolic higher-order shear deformation plate formulation based on modified radial distance based MQ-RBF meshfree method is considered for the flexural analysis of FGM plate. Eight types of distributed transverse loads for the bending analysis of elastically supported porous FGM plate have been considered. We concluded that the results obtained by the present solution methodology are in good agreement with other published results. These are some of the primary present study conclusions.

- The stability and results of the present formulation using MQ-RBF are in good agreement with other published results, which shows its applicability.
- With the increase in the grading index, normalized deflection also increases, and this effect becomes insignificant if the grading index is increased for more than 5.
- The normalized deflection increases by increasing the porosity fraction. The effect of P decreases when plates become thick to thin.
- The effect of P is more in the metal phase than the ceramic phase.
- With the increase in a/b, the normalized deflection decreases.
- The effects of Ks are prominent as compared to Kw.
- Some new results for porous FGM plates resting on the elastic foundation are presented, which can be used for further validation and research.

The present result may be a benchmark for further examination of FGM plates resting on an elastic foundation.

Conflicts of Interest

The author declares that there is no conflict of interest regarding the publication of this manuscript.

Appendix -I

The GDEs are expressed in terms of displacement components and are represented as:

$$\left(A_{11} \frac{\partial^2 u_0}{\partial x^2} + A_{66} \frac{\partial^2 u_0}{\partial y^2} \right) + \left(A_{12} \frac{\partial^2 v_0}{\partial x \partial y} + A_{66} \frac{\partial^2 v_0}{\partial x \partial y} \right) + \left(-B_{11} \frac{\partial^3 w_0}{\partial x^3} - B_{12} \frac{\partial^3 w_0}{\partial x \partial y^2} - 2B_{66} \frac{\partial^3 w_0}{\partial x \partial y^2} \right) \tag{34}$$

$$+ \left(E_{11} \frac{\partial^2 \phi_x}{\partial x^2} + E_{66} \frac{\partial^2 \phi_x}{\partial y^2} \right) + \left(E_{12} \frac{\partial^2 \phi_y}{\partial x \partial y} + E_{66} \frac{\partial^2 \phi_y}{\partial x \partial y} \right) = 0$$

$$\left(A_{66} \frac{\partial^2 u_0}{\partial x \partial y} + A_{12} \frac{\partial^2 u_0}{\partial x \partial y} \right) + \left(A_{66} \frac{\partial^2 v_0}{\partial x^2} + A_{22} \frac{\partial^2 v_0}{\partial y^2} \right) + \left(-2B_{66} \frac{\partial^3 w_0}{\partial x^2 \partial y} - B_{12} \frac{\partial^3 w_0}{\partial x^2 \partial y} - B_{22} \frac{\partial^3 w_0}{\partial y^3} \right) \tag{35}$$

$$+ \left((E_{12} + E_{66}) \frac{\partial^2 \phi_x}{\partial x \partial y} \right) + \left(+E_{66} \frac{\partial^2 \phi_y}{\partial x^2} + E_{22} \frac{\partial^2 \phi_y}{\partial y^2} \right) = 0$$

$$\left(B_{11} \frac{\partial^3 u_0}{\partial x^3} + (B_{12} + 2B_{66}) \frac{\partial^3 u_0}{\partial x \partial y^2} \right) + \left(B_{22} \frac{\partial^3 v_0}{\partial y^3} + (B_{12} + 2B_{66}) \frac{\partial^3 v_0}{\partial x^2 \partial y} \right)$$

$$- \left(D_{11} \frac{\partial^4 w_0}{\partial x^4} + (2D_{12} + 4D_{66}) \frac{\partial^4 w_0}{\partial x^2 \partial y^2} + D_{22} \frac{\partial^4 w_0}{\partial y^4} \right) \tag{36}$$

$$+ \left(F_{11} \frac{\partial^3 \phi_x}{\partial x^3} + (F_{12} + 2F_{66}) \frac{\partial^3 \phi_x}{\partial x \partial y^2} \right)$$

$$+ \left(F_{22} \frac{\partial^3 \phi_y}{\partial y^3} + (F_{12} + 2F_{66}) \frac{\partial^3 \phi_y}{\partial x^2 \partial y} \right)$$

$$- K w w_0 + K s \left(\frac{\partial^2 w_0}{\partial x^2} + \frac{\partial^2 w_0}{\partial x^2} \right) = q$$

$$\left(E_{11} \frac{\partial^2 u_0}{\partial x^2} + E_{66} \frac{\partial^2 u_0}{\partial y^2} \right) + \left(E_{12} \frac{\partial^2 v_0}{\partial x \partial y} + E_{66} \frac{\partial^2 v_0}{\partial x \partial y} \right)$$

$$+ \left(-F_{11} \frac{\partial^3 w_0}{\partial x^3} - (F_{12} + 2F_{66}) \frac{\partial^3 w_0}{\partial x \partial y^2} \right) \tag{37}$$

$$+ \left(H_{11} \frac{\partial^2 \phi_x}{\partial x^2} + H_{66} \frac{\partial^2 \phi_x}{\partial y^2} - A_{55} \phi_x \right) +$$

$$\left((H_{12} + H_{66}) \frac{\partial^2 \phi_y}{\partial x \partial y} + H_{22} \frac{\partial^2 \phi_y}{\partial y^2} \right) = 0$$

$$\left(E_{66} \frac{\partial^2 u_0}{\partial x \partial y} + E_{12} \frac{\partial^2 u_0}{\partial x \partial y} \right)$$

$$+ \left(+E_{66} \frac{\partial^2 v_0}{\partial x^2} + E_{22} \frac{\partial^2 v_0}{\partial y^2} \right)$$

$$+ \left(-(F_{12} + F_{66}) \frac{\partial^3 w_0}{\partial y \partial x^2} - F_{22} \frac{\partial^3 w_0}{\partial y^3} \right) \tag{38}$$

$$+ \left(H_{66} \frac{\partial^2 \phi_x}{\partial x \partial y} + H_{12} \frac{\partial^2 \phi_x}{\partial x \partial y} \right) +$$

$$\left(H_{66} \frac{\partial^2 \phi_y}{\partial x^2} + H_{22} \frac{\partial^2 \phi_y}{\partial y^2} - A_{44} \phi_y \right) = 0$$

Appendix -II

The first part of GDEs (5) $\delta u_0 : \frac{\partial N_{xx}}{\partial x} + \frac{\partial N_{xy}}{\partial y} = 0$

are discretized using MQ-RBF and are expressed as:

$$[K'_{1u}]_{(NI,N)} = \sum_{i=1}^{NI} \sum_{j=1}^N \left(A_{11} \frac{\partial^2 g_{(i,j)}}{\partial x^2} + A_{66} \frac{\partial^2 g_{(i,j)}}{\partial y^2} + 2A_{16} \frac{\partial^2 g_{(i,j)}}{\partial x \partial y} \right) \tag{39}$$

$$[K'_{1v}]_{(NI,N)} = \sum_{i=1}^{NI} \sum_{j=1}^N \left(A_{12} \frac{\partial^2 g_{(i,j)}}{\partial x \partial y} + A_{16} \frac{\partial^2 g_{(i,j)}}{\partial x^2} + A_{66} \frac{\partial^2 g_{(i,j)}}{\partial x \partial y} + A_{26} \frac{\partial^2 g_{(i,j)}}{\partial y^2} \right) \tag{40}$$

$$[K'_{1w}]_{(NI,N)} = \sum_{i=1}^{NI} \sum_{j=1}^N \left(-B_{11} \frac{\partial^3 g_{(i,j)}}{\partial x^3} - B_{12} \frac{\partial^3 g_{(i,j)}}{\partial x \partial y^2} - 3B_{16} \frac{\partial^3 g_{(i,j)}}{\partial x^2 \partial y} - 2B_{66} \frac{\partial^3 g_{(i,j)}}{\partial x \partial y^2} - B_{26} \frac{\partial^3 g_{(i,j)}}{\partial y^3} \right) \tag{41}$$

$$[K'_{1\phi_x}]_{(NI,N)} = \sum_{i=1}^{NI} \sum_{j=1}^N \left(E_{11} \frac{\partial^2 g_{(i,j)}}{\partial x^2} + 2E_{16} \frac{\partial^2 g_{(i,j)}}{\partial x \partial y} + E_{66} \frac{\partial^2 g_{(i,j)}}{\partial y^2} \right) \tag{42}$$

$$[K'_{1\phi_y}]_{(NI,N)} = \sum_{i=1}^{NI} \sum_{j=1}^N \left(E_{12} \frac{\partial^2 g_{(i,j)}}{\partial x \partial y} + E_{16} \frac{\partial^2 g_{(i,j)}}{\partial x^2} + E_{26} \frac{\partial^2 g_{(i,j)}}{\partial y^2} + E_{66} \frac{\partial^2 g_{(i,j)}}{\partial x \partial y} \right) \tag{43}$$

Similarly, other parts of GDEs are discretized.

The boundary conditions can be discretized similarly. E.g., simply supported boundary condition at the edge $x=0$ (equation -8) is discretized and finally expressed as:

$$[K]_{b,x=0} \{\delta\} = \{0\} \tag{44}$$

$$[K]_{b,x=0} = \begin{bmatrix} [K'_{1u}] & [K'_{1v}] & [K'_{1w}] & [K'_{1\phi_x}] & [K'_{1\phi_y}] \\ [0]_{nbx_0 \times N} & [K'_{2v}] & [0]_{nbx_0 \times N} & [0]_{nbx_0 \times N} & [0]_{nbx_0 \times N} \\ [0]_{nbx_0 \times N} & [K'_{2v}] & [K'_{3w}] & [0]_{nbx_0 \times N} & [0]_{nbx_0 \times N} \\ [K'_{4u}] & [K'_{4v}] & [K'_{4w}] & [K'_{4\phi_x}] & [K'_{4\phi_y}] \\ [0]_{nbx_0 \times N} & [K'_{2v}] & [0]_{nbx_0 \times N} & [0]_{nbx_0 \times N} & [K'_{5\phi_y}] \end{bmatrix} \tag{45}$$

nbx_0 = number of nodes on the boundary $x=0$.

$$[K^{lb}_{1u}] = \sum_{i=NI+1}^{NI+1+nbx_0} \sum_{j=1}^N \left(A_{11} \frac{\partial g_{(i,j)}}{\partial x} + A_{16} \frac{\partial g_{(i,j)}}{\partial y} \right) \tag{46}$$

$$[K^{lb}_{1v}] = \sum_{i=NI+1}^{NI+1+nbx_0} \sum_{j=1}^N \left(A_{12} \frac{\partial g_{(i,j)}}{\partial x} + A_{16} \frac{\partial g_{(i,j)}}{\partial y} \right) \tag{47}$$

$$[K^{lb}_{1\phi_x}] = \sum_{i=NI+1}^{NI+1+nbx_0} \sum_{j=1}^N \begin{pmatrix} -B_{11} \frac{\partial^2 g_{(i,j)}}{\partial x^2} - B_{12} \frac{\partial^2 g_{(i,j)}}{\partial y^2} \\ -2B_{16} \frac{\partial^2 g_{(i,j)}}{\partial y \partial x} \end{pmatrix} \quad (48)$$

$$[K^l_{1\phi_x}] = \sum_{i=NI+1}^{NI+1+nbx_0} \sum_{j=1}^N \left(E_{12} \frac{\partial g_{(i,j)}}{\partial y} + E_{16} \frac{\partial g_{(i,j)}}{\partial x} \right) \quad (49)$$

$$[K^{lb}_{1\phi_y}] = \sum_{i=NI+1}^{NI+1+nbx_0} \sum_{j=1}^N \left(E_{11} \frac{\partial g_{(i,j)}}{\partial x} + E_{16} \frac{\partial g_{(i,j)}}{\partial y} \right) \quad (50)$$

$$[K^{lb}_{2v}] = \sum_{i=NI+1}^{NI+1+nbx_0} \sum_{j=1}^N g_{(i,j)} \quad (51)$$

$$[K^{lb}_{3w}] = \sum_{i=NI+1}^{NI+1+nbx_0} \sum_{j=1}^N g_{(i,j)} \quad (52)$$

$$[K^{lb}_{4u}] = \sum_{i=NI+1}^{NI+1+nbx_0} \sum_{j=1}^N \left(B_{11} \frac{\partial g_{(i,j)}}{\partial x} + B_{16} \frac{\partial g_{(i,j)}}{\partial y} \right) \quad (53)$$

$$[K^{lb}_{4v}] = \sum_{i=NI+1}^{NI+1+nbx_0} \sum_{j=1}^N \left(B_{12} \frac{\partial g_{(i,j)}}{\partial x} + B_{16} \frac{\partial g_{(i,j)}}{\partial y} \right) \quad (54)$$

$$[K^{lb}_{4w}] = \sum_{i=NI+1}^{NI+1+nbx_0} \sum_{j=1}^N \begin{pmatrix} -D_{11} \frac{\partial^2 g_{(i,j)}}{\partial x^2} - D_{12} \frac{\partial^2 g_{(i,j)}}{\partial y^2} \\ -2D_{16} \frac{\partial^2 g_{(i,j)}}{\partial y \partial x} \end{pmatrix} \quad (55)$$

$$[K^l_{4\phi_x}] = \sum_{i=NI+1}^{NI+1+nbx_0} \sum_{j=1}^N \left(F_{12} \frac{\partial g_{(i,j)}}{\partial y} + F_{16} \frac{\partial g_{(i,j)}}{\partial x} \right) \quad (56)$$

$$[K^{lb}_{4\phi_y}] = \sum_{i=NI+1}^{NI+1+nbx_0} \sum_{j=1}^N \left(F_{11} \frac{\partial g_{(i,j)}}{\partial x} + F_{16} \frac{\partial g_{(i,j)}}{\partial y} \right) \quad (57)$$

$$[K^{lb}_{5\phi_y}] = \sum_{i=NI+1}^{NI+1+nbx_0} \sum_{j=1}^N g_{(i,j)} \quad (58)$$

Similarly, other boundary conditions at the edges $x=a$, $y=0$, and $y=b$ are discretized. The resulting equation is written in matrix form as:

$$[K]_B \{\delta\} = \{0\} \quad (59)$$

where

$$[K]_B = \left[\left[[K]_{b,y=0} [K]_{b,x=a} [K]_{b,y=b} [K]_{b,x=0} \right]_{(5 \times N_b, 5 \times N)} \right]^T \quad (60)$$

References

[1] Chen J.-S., Hillman M., Chi S.-W., 2017. Meshfree Methods: Progress Made after 20 Years. *Journal of Engineering Mechanics*, 143(4), pp.04017001.
 [2] Kansa E.J., 1990. Multiquadrics—A scattered data approximation scheme with applications to computational fluid-dynamics—I surface approximations and partial derivative estimates. *Computers & Mathematics with Applications*, 19(8), pp.127-145.

[3] Kansa E.J., 1990. Multiquadrics—A scattered data approximation scheme with applications to computational fluid-dynamics—II solutions to parabolic, hyperbolic and elliptic partial differential equations. *Computers & Mathematics with Applications*, 19(8), pp.147-161.
 [4] Wang J.G., Liu G.R., 2002. A point interpolation meshless method based on radial basis functions. *International Journal for Numerical Methods in Engineering*, 54(11), pp.1623-1648.
 [5] Hardy R.L., 1971. Multiquadric equations of topography and other irregular surfaces. *Journal of Geophysical Research*, (1896-1977) 76(8), pp.1905-1915.
 [6] Franke R., 1982. Scattered data interpolation: tests of some methods. *Mathematics of Computation*, 38(157), pp.181-200.
 [7] Carrera E., Brischetto S., Robaldo A., 2008. Variable Kinematic Model for the Analysis of Functionally Graded Material plates. *AIAA Journal*, 46(1), pp.194-203.
 [8] Zenkour A.M., 2006. Generalized shear deformation theory for bending analysis of functionally graded plates. *Applied Mathematical Modelling*, 30(1), pp. 67-84.
 [9] Mantari J.L., Oktem A.S., Guedes Soares C., 2012. Bending response of functionally graded plates by using a new higher order shear deformation theory. *Composite Structures*, 94(2), pp.714-723.
 [10] Kumar R., Lal A., Singh B.N., Singh J., 2019. New transverse shear deformation theory for bending analysis of FGM plate under patch load. *Composite Structures*, 208, pp.91-100.
 [11] Neves A.M.A., Ferreira A.J.M., Carrera E., Roque C.M.C., Cinefra M., Jorge R.M.N., et al. 2011. Bending of FGM plates by a sinusoidal plate formulation and collocation with radial basis functions. *Mechanics Research Communications*, 38(5), 368-371.
 [12] Mechab I., Atmane H.A., Tounsi A., Belhadj H.A., Bedia E.A.A., 2010. A two-variable refined plate theory for the bending analysis of functionally graded plates. *Acta Mechanica Sinica*, 26(6), pp.941-949.
 [13] Vafakhah Z., Navayi Neya B., 2019. An exact three-dimensional solution for bending of thick rectangular FGM plate. *Composites Part B: Engineering* 156, pp.72-87.
 [14] Meksi A., Benyoucef S., Houari M.S.A., Tounsi A., 2015. A simple shear deformation theory based on the neutral surface position for functionally graded plates resting on Pasternak elastic foundations. *Structural Engineering and Mechanics*, 53, pp.1215-1240.

- [15] Yahia SA, Atmane HA, Houari MSA, Tounsi A. 2015. Wave propagation in functionally graded plates with porosities using various higher-order shear deformation plate theories. *Structural Engineering and Mechanics*, 53(6), 1143–1165.
- [16] Benferhat R., Hassaine Daouadji T., Hadji L., Said Mansour M., 2016. Static analysis of the FGM plate with porosities. *Steel and Composite Structures*, 21(1), pp. 123–136.
- [17] Kim J., Žur K.K., Reddy J.N., 2019. Bending, free vibration and buckling of modified couples stress-based functionally graded porous micro-plates. *Composite Structures*, 209, 879–888.
- [18] Akbaş Ş.D., 2017. Vibration and Static Analysis of Functionally Graded Porous Plates. *Journal of Applied and Computational Mechanics*, 3(3), pp. 199–207.
- [19] Mechab I., Mechab B., Benaissa S., Serier B., Bouiadjra B.B., 2016. Free vibration analysis of FGM nanoplate with porosities resting on Winkler Pasternak elastic foundations based on two-variable refined plate theories. *Journal of the Brazilian Society of Mechanical Sciences and Engineering*, 38(8), pp.2193–2211.
- [20] Gupta A., Talha M., 2018. Influence of porosity on the flexural and vibration response of gradient plate using nonpolynomial higher-order shear and normal deformation theory. *International Journal of Mechanics and Materials in Design*, 14(2), 277–296.
- [21] Rezaei A.S, Saidi A.R, Abrishamdari M, Mohammadi M.H.P., 2017. Natural frequencies of functionally graded plates with porosities via a simple four variable plate theory: An analytical approach. *Thin-Walled Structures*, 120, pp. 366–377.
- [22] Chen D., Yang J., Kitipornchai S., 2019. Buckling and bending analyses of a novel functionally graded porous plate using the Chebyshev-Ritz method. *Archives of Civil and Mechanical Engineering*, 19(1), pp.157–170.
- [23] Solanki M. K., Kumar R., and Singh J., 2018. Flexure Analysis of Laminated Plates Using Multiquadratic RBF Based Meshfree Method. *International Journal of Computational Methods*, 15(06), pp. 1850049
- [24] Ferreira A.J.M., Batra. R.C., Roque C.M.C., Qian L.F., Martins P.A.L.S., 2005. Static analysis of functionally graded plates using third-order shear deformation theory and a meshless method. *Composite Structures*, 69(4), pp. 449–457.
- [25] Dai K.Y., Liu G.R., Lim K.M., Han X., Du S.Y., 2004. A mesh-free radial point interpolation method for analysis of functionally graded material (FGM) plates. *Computational Mechanics* 34(3) pp. 213–223.
- [26] Wu C-P., Chiu K-H., Wang Y-M., 2011. RMVT-based meshless collocation and element-free Galerkin methods for the quasi-3D analysis of multilayered composite and FGM plates. *Composite Structures*, 93, pp.1433–1448.
- [27] Neves A.M.A., Ferreira A.J.M., Carrera E., Roque C.M.C., Cinefra M., Jorge R.M.N., et al. 2012. A quasi-3D sinusoidal shear deformation theory for the static and free vibration analysis of functionally graded plates. *Composites Part B: Engineering*, 43(2), pp.711–725.
- [28] Xiang S., Kang G., 2013. An nth-order shear deformation theory for the bending analysis on the functionally graded plates. *European Journal of Mechanics - A/Solids*, 37, pp.336–343.
- [29] Xiang S, Kang G., 2013. Static analysis of functionally graded plates by the various shear deformation theory. *Composite Structures*, 99, pp. 224–230.
- [30] Kumar R., Lal A., Singh B.N., Singh J., 2019. Meshfree approach on buckling and free vibration analysis of porous FGM plate with proposed IHSDT resting on the foundation. *Curved and Layered Structures* 6(1),192–211.
- [31] Singh J., Singh S., Shukla K.K., 2014. Meshless Analysis of Laminated Composite and Sandwich Plates Subjected to Various Types of Loads. *International Journal for Computational Methods in Engineering Science and Mechanics*,15, pp.158–171.
- [32] Kumar R., Singh J., 2018. Assessment of higher order transverse shear deformation theories for modeling and buckling analysis of FGM plates using RBF-based meshless approach. *Multidiscipline Modeling in Materials and Structures*, 14, pp. 891-907.
- [33] Kumar R., Lal A., Singh B.N., Singh J., 2020. Non-linear analysis of porous elastically supported FGM plate under various loading. *Composite Structures*, 233, pp. 111721.
- [34] Akavci S.S., 2014. An efficient shear deformation theory for free vibration of functionally graded thick rectangular plates on elastic foundation. *Composite Structures*, 108, pp.667–676.
- [35] Daikh A.A., 2019 Temperature-dependent vibration analysis of functionally graded sandwich plates resting on Winkler/Pasternak/Kerr foundation. *Materials Research Express*, 6, pp.065702.
- [36] Kumar R., Lal A., Singh BN., Singh J., 2021. Numerical simulation of the thermomechanical buckling analysis of bidirectional porous functionally graded plate using collocation meshfree method.

- Proceedings of the Institution of Mechanical Engineers, Part L, 236(4), pp.787-807.
- [37] Wu C-P., Chiu K-H., 2011. RMVT-based meshless collocation and element-free Galerkin methods for the quasi-3D free vibration analysis of multilayered composite and FGM plates. *Composite Structures*, 93, 1433–1448.
- [38] Wu C-P., Li H-Y., 2010. An RMVT-based third-order shear deformation theory of multilayered functionally graded material plates. *Composite Structures*, 92, 2591–2605.
- [39] Thai H-T., Kim S-E., 2013. A simple higher-order shear deformation theory for bending and free vibration analysis of functionally graded plates. *Composite Structures*, 96, pp. 165–173.